Astronomy 218
Haystack Observatory Project Report
Data taken Nov. 1, 2007
Final submission Jan. 28, 2008

Sarah Ballard, Robert Harris, Lauranne Lanz, Bennett Maruca, and Diego Muñoz

Harvard-Smithsonian Center for Astrophysics, 60 Garden Street, Cambridge, MA 02138

Contents

1 Calibration and Measurements with a 7.5-Foot Radio Telescope at 1420 MHz (led by Ben Maruca and Diego Munoz) 4

1.1 Receiver Temperature . . . 4
1.2 Beam-Width . . . 6
1.3 Antenna Temperature . . . 7
1.4 Aperture Efficiency . . . 7
1.4.1 Numerical Evaluation . . . 8
1.4.2 Analytical Evaluation . . . 8
1.5 Expected Solar Flux Density . . . 10
1.6 Galactic Rotation Curve . . . 10
1.6.1 The Data . . . 15

2 Haystack Project 2: Angular Size of the Sun (led by Sarah Ballard) 18

2.1 Calculating the projected baseline length . . . 18
2.2 The effect of the finite bandwidth on the fringe visibility . . . 19
2.3 Fitting to the function of a uniformly bright disk . . . 20
2.4 Effects of limb brightening . . . 21
2.5 Fitting parameters vs. inverse Hankel transform . . . 24

3 Haystack Project 3: Measurements of the Visibility of a Single and Double Source (led by Robert Harris and Lauranne Lanz) 24

3.1 Theory of Two-Element Interferometry . . . 25
3.2 Experimental Setup and Procedures . . . 27

3.3 Data and Analysis 28
3.3.1 Measurement of Single Source Visibility 28
3.3.2 Measuring the Visibility as a Function of Baseline Separation 30
3.3.3 Measuring the Visibility as a Function of Source Separation 32
3.4 Discussion of Results 32

4 APPENDIX 1 **35**
4.1 Projects for the Haystack Trip 35

5 APPENDIX 2 **39**
5.1 Guidelines for report on measurements made at Haystack on Nov 1, 2007 39
5.2 PROJECT 1. Calibration and Measurements with a 7.5 ft radio telescope at 1420 MHz. 39
5.3 PROJECT 2. Measure the angular size of the sun with the two element interferometer. 40
5.4 PROJECT 3. Measure the visibility function of a simulated double source made from two florescent lights. 42

List of Tables

1 Various choices for $T_{\rm abs}$, $T_{\rm atm}$, and $T_{\rm cal}$ that are consistent with Equation (5). 5
2 Ben and Diego's Galactic Rotation Curve Data 16
3 Robert and Claude-Andre's Galactic Rotation CurveData 16
4 Frequency Determinations from Each of the 3 Experiment Phases 34

List of Figures

1 The brightness temperature of the Sun as a function of distance from the the center for select wavelengths [3]. 11
2 The mean brightness temperature of the Sun as a function of wavelength (thick curve) against black-bodies at various temperatures [3]. 12
3 Galactic differential rotation. For each line of sight in the first and fourth quadrants in galactic coordinates (l, b) – i.e. the inner Galaxy – two points with the same linear velocity and the same distance from the Galactic Center are intercepted. Without auxiliary distance indicators, these two points are indistinguishable, introducing an ambiguity. 13

4 Geometry of the distance ambiguity. For a given line of sight – angle l – two points at different distances will be observed to have the same projected velocity. 14

5 Line of sight reaching tangentially the ring of radius R. 15

6 Observing in the Galactic second quadrant. 17

7 Rotation curve from Table 2 excluding observations beyond a longitude of 90°. . . . 18

8 Rotation curve from Table 3 excluding observations beyond a longitude of 90° 19

9 Projected baseline versus time, for useable observations. 20

10 The best fit visibility function with data overplotted. The best fit angular size of the sun was measured to be 33.2', about 3% larger than the optical angular size of 32.3'. 22

11 The bestfit visibility function with the extra limb brightening term (at a fraction of 25% of the disk intensity), just to compare their behaviors. 23

12 Inset of best-fit visibility function, with maximum limb brightening contribution (at 5%) overplotted. It's clear that a limb brightening fraction any higher would be inconsistent with the observations. 24

13 Illustration of the plane of the sky when observing a double source. 26

14 Circuit diagram for project 3. Obtained from VSRT Memo 025. 27

15 Measured and fit visibilities for a single fluorescent lamp. The top plot, (a), gives the measured (crosses with errors) and fit (solid line) power expressed in Kelvin as a function of baseline separation. The bottom plot, (b), gives the residuals of the fit expressed in terms of the estimated error on the measurements. 30

16 The top plot, (a), gives the measured (crosses with error bars) and fit (solid line) uncalibrated powers for a double source as a function of baseline separation. The bottom plot, (b), gives the residuals of the fit expressed. 31

17 Measurement of the visibility of the double source as a function of source separation. The top plot, (a), gives the measured (crosses and error bars) and fit (straight line) uncalibrated powers for a double source as a function of source separation. The bottom plot, (b), gives the residuals of the fit. 33

1. Calibration and Measurements with a 7.5-Foot Radio Telescope at 1420 MHz (led by Ben Maruca and Diego Munoz)

1.1. Receiver Temperature

We had at our disposal, two separate calibration schemes. For the first of these, the "calibrated load" method, we pointed the dish to an "empty" part of the sky. Though the antenna was not directed to any particular source, power P was still measured from the atmosphere (T_{atm}) and from the receiver (T_{rec}). We then electronically added into the signal power from a calibrated load that had a temperature T_C and measured the power that it added to the overall signal, P_{cal}. Since the system was not calibrated, any measurements of power (an subsequently temperature) were in arbitrary and unknown units. Therefore, we could only reliable measure the ratio of these two powers:

$$y_c = \frac{P}{P_{\text{cal}}} = \frac{T_{\text{rec}} + T_{\text{atm}}}{T_{\text{cal}}} \ . \tag{1}$$

In particular, we measured $y_c = 1.01$.

For the second calibration scheme, the "absorber" method, we again began by measuring the power P when the dish was directed at empty sky. Recall that P is the sum of power from the atmosphere at a temperature T_{atm} and that from the receiver at a temperature T_{rec}. We then introduced a thick block of absorbent foam between the antenna's dish and its feed. In this case, power from the receiver is still collected while that from the atmosphere is blocked by the foam. Instead, the total power measured (P_{abs}) is the sum of the power from the receiver and that from the foam. We assumed that the foam was a thermal emitter at a temperature T_{abs}. Since, as before, the units of power in an uncalibrated system have no physical meaning, we could only measure the ratio of these two powers:

$$y_a = \frac{P_{\text{abs}}}{P} = \frac{T_{\text{rec}} + T_{\text{abs}}}{T_{\text{rec}} + T_{\text{atm}}} \ . \tag{2}$$

By measuring system temperature both with the foam removed and inserted, we found that $y_a = 2.48$.

Solving Equations (1) and (2) each for the receiver temperature gives

$$\begin{cases} T_{\text{rec}} = y_c T_{\text{cal}} - T_{\text{atm}} \\ T_{\text{rec}} = \frac{T_{\text{abs}} - y_a T_{\text{atm}}}{y_a - 1} \end{cases} \ . \tag{3}$$

If we assume that both of these methods are equally reliable, then we may equate these two expressions as follows:

$$y_c \ (y_a - 1) \ T_{\text{cal}} + T_{\text{atm}} = T_{\text{abs}} \ . \tag{4}$$

The substitution of our measured values of y_c and y_a gives

$$1.48 \ T_{\text{cal}} + T_{\text{atm}} = T_{\text{abs}} \ . \tag{5}$$

From this expression, it is clear that the receiver temperature $T_{\rm rec}$ can only be inferred if two of the following values are known in physical units: $T_{\rm abs}$, $T_{\rm atm}$, and $T_{\rm cal}$. Unfortunately, we have limited information on these three quantities. If the absorber were perfect, then $T_{\rm abs}$ would be approximately the ambient temperature, which was about 295 K. However, since a perfect absorber does not exist, the value of 295 K is only an upper bound to $T_{\rm abs}$. The effective atmospheric temperature, $T_{\rm atm}$, is likewise difficult to discern since it depends on variations in weather and the elevation-angle of the dish. However, at wavelengths near $\lambda_0 = 21$ cm, $T_{\rm atm}$ is known to range from about 0 K to about 30 K. Finally, while we were informed that $T_{\rm cal}$ was about 100 K, but we were not provided with a more exact value and were not able to measure the value of $T_{\rm cal}$ ourselves.

Table 1 gives sets of values of $T_{\rm abs}$, $T_{\rm atm}$, and $T_{\rm cal}$ that satisfy Equation (5) and are consistent with the limited information that we have about each quantity as stated above. In fact, there is quite a wide range of values for each of these three temperatures, which corresponds to a problematically wide range is possible values for the receiver temperature (Equation 3). Given that so many of the following calculations rely directly on the receiver temperature, we decided to choose "reasonable" values for $T_{\rm abs}$, $T_{\rm atm}$, and $T_{\rm cal}$ and to use these to solve from $T_{\rm rec}$. While this gives a value of $T_{\rm rec}$ that is not exact, it does give a value that is "typical" and useful for assessing the system's general performance.

Table 1: Various choices for $T_{\rm abs}$, $T_{\rm atm}$, and $T_{\rm cal}$ that are consistent with Equation (5).

	$T_{\rm atm} = 0$ K	$T_{\rm atm} = 30$ K
$T_{\rm cal}$	$T_{\rm abs}$	$T_{\rm abs}$
50 K	74 K	104 K
75 K	111 K	141 K
100 K	148 K	178 K
125 K	185 K	215 K
150 K	222 K	252 K
175 K	259 K	289 K

We assume that the absorber, though not perfect, was significantly opaque. Subsequently, we required that $T_{\rm cal} \gtrsim 100$ K so that $T_{\rm abs}$ is not too far below the ambient temperature of about 295 K. In this regime, both $T_{\rm abs}$ and $T_{\rm cal}$ are large enough that the value of $T_{\rm atm}$ does not have a great effect on $T_{\rm rec}$. Therefore, for simplicity, we assumed that

$$\begin{cases} T_{\rm abs} = 222 \text{ K} \\ T_{\rm atm} = 0 \text{ K} \\ T_{\rm cal} = 150 \text{ K} \end{cases}, \tag{6}$$

which corresponds to a virtually transparent atmosphere and an absorber that is about $222/295 =$

75.3% opaque. Substitution of these values into Equation (3) gives a receiver temperature of

$$T_{\rm rec} = 152 \text{ K} . \tag{7}$$

Note that we use this value in all subsequent calculations for which the receiver temperature is relevant.

1.2. Beam-Width

We used the provided software to analyze data from a five-by-five-observation raster scan across the Sun and find that the beam-width (full-width at half-maximum) of the antenna is $5.2^{\rm o}$ in azimuth and $6.0^{\rm o}$ in elevation.

Of course, this software does have its limitation, which become apparent when one investigates the mathematical basis of its algorithms. In general, a single-dish antenna has some (two-dimensional) beam-pattern. Likewise, a sky object has an angle-dependent brightness-distribution. Assuming that the beam-pattern is stable (e.g., independent of elevation angle), the system power as a function of sky angle is simply the convolution of the antenna's beam-pattern with the object's brightness-distribution. The software, in fact, used a raster scan to measure the system power at different angles, fit these measurements to a Gaussian distribution, and took the width of this distribution along each axis (i.e., azimuth and elevation) to be the beam-width of the antenna. Even assuming that the beam-pattern of the antenna is well modeled by a Gaussian distribution, this technique implicitly assumes that the source under observation is a point-source; it is only under this condition that the beam-pattern is proportional to the angular distribution of system power. When we analyzed the Sun with this software, was tacitly treated the Sun as a point source. As the Sun in fact has a non-zero angular width of about $0.5^{\rm o}$, it is important to understand what impact this assumption has had on our measurements.

Assume that both the beam-pattern of the antenna and the brightness-distribution of the source (i.e., the Sun) are well-modeled by Gaussian distributions with widths (along any one axis) of θ_b and θ_S. Note that the particular definition of "width" (e.g., full-width at half-maximum) does not matter so long as it is proportional to the standard-deviation of the Gaussian distribution. Our raster scan measured the system power as a function of angular position on the sky, which is simply a convolution of the beam-pattern and brightness-distribution. Note that two Gaussian distributions convolve into yet another Gaussian distribution with a standard deviation that is the quadrature sum of those of the original distributions. Thus,

$$\theta_m = \sqrt{\theta_b^2 + \theta_S^2} , \tag{8}$$

where θ_m is the width of the system-power angular-distribution. While we are actually wish to measure the beam-width θ_b, the software actually outputs θ_m. Assuming that θ_b and θ_m are both

significantly larger than θ_S,

$$\theta_m = \theta_b \sqrt{1 + \frac{\theta_S^2}{\theta_b^2}} \approx \theta_b + \frac{\theta_S^2}{2\theta_b} \ . \tag{9}$$

Thus, the difference between the measured and actual beam-widths is about

$$\Delta_\theta := \theta_m - \theta_b \approx \frac{\theta_S^2}{2\theta_b} \ . \tag{10}$$

This corresponds to a fractional error

$$\frac{\Delta_\theta}{\theta_b} \approx \frac{\theta_S^2}{2\theta_b^2} \ . \tag{11}$$

To evaluate this expression for Δ_θ, we assume that $\theta_S = 0.5^{\rm o}$. Likewise, we assume that $\theta_b \approx \theta_m$ and use our measured values of $\theta_b \approx \theta_m = 5.2^{\rm o}$ in azimuth and $\theta_b \approx \theta_m = 6.0^{\rm o}$ in elevation. Therefore, the software's treatment of the Sun as a point-source introduced a 0.46% error to the azimuth beam-width and a 0.35% error to the elevation beam width.

1.3. Antenna Temperature

Let $T_{\rm Sun}$ be the the system temperature with the dish pointed directly at the Sun. Therefore,

$$T_{\rm Sun} = T_{\rm ant} + T_{\rm rec} \ , \tag{12}$$

where $T_{\rm ant}$ is the antenna temperature resulting from this observation. Since we observed $T_{\rm Sun}$ to be 3.1 $T_{\rm cal}$, then using the assumed values for $T_{\rm cal}$ and $T_{\rm rec}$ from above,

$$\begin{aligned} T_{\rm ant} &= 3.1\ T_{\rm cal} - T_{\rm rec} = (3.1)\,(150\ {\rm K}) - (152\ {\rm K}) \\ T_{\rm ant} &= 313\ {\rm K} \ . \end{aligned} \tag{13}$$

1.4. Aperture Efficiency

The on-axis, geometric area of the aperture is

$$\begin{aligned} A_g &= \pi \left(\tfrac{7.5\ {\rm ft}}{2}\right)^2 \left(\tfrac{1\ {\rm m}}{3.28\ {\rm ft}}\right)^2 \\ A_g &= 4.11\ {\rm m}^2 \ . \end{aligned} \tag{14}$$

Let $A(\alpha, \beta)$ be the effective collecting area of the dish where (α, β) the the sky position relative to the pointing center. We assume that $A(\alpha, \beta)$ is a two-dimensional Gaussian distribution so that

$$A(\alpha, \beta) = \eta\ A_g\ e^{-(\log 2)\left(\frac{\alpha^2}{\alpha_w^2} + \frac{\beta^2}{\beta_w^2}\right)} \ , \tag{15}$$

where η is the aperture efficiency and $\alpha_w = 2.6^{\rm o} = 0.0454$ and $\beta_w = 3.0^{\rm o} = 0.0524$ are the measured half-widths at half-maximum of the beam-pattern. Assume that the brightness-distribution of the Sun is a uniform disc of angular radius $\gamma_S = 0.25^{\rm o} = 0.00436$. Therefore, the antenna temperature corresponding to the pointing of the dish directly at the Sun is (1)

$$T_{\rm ant} = \frac{S}{\pi \gamma_S^2} \, \frac{1}{2 \, k_B} \int \int_{\rm Sun} A(\alpha, \beta) \, d\beta \, d\alpha \ , \tag{16}$$

where this integral is taken over the disc of the Sun and $S = 5.4 \times 10^{-21}$ W/m^2/Hz $= 5.4 \times 10^{-21}$ J/m^2 is the solar flux density measured by the National Oceanic and Atmospheric Administration (NOAA) (2) on that day. Note that this equation has made implicit use of the Rayleigh-Jeans approximation. By substitution,

$$\begin{aligned} T_{\rm ant} &= \frac{S \ \eta \ A_g}{2 \ \pi \ \gamma_S^2 \ k_B} \ \int_{-\gamma_S}^{\gamma_S} \int_{-\sqrt{\gamma_S^2 - \alpha^2}}^{\sqrt{\gamma_S^2 - \alpha^2}} e^{-(\log 2) \left(\frac{\alpha^2}{\alpha_w^2} + \frac{\beta^2}{\beta_w^2} \right)} \, d\beta \, d\alpha \\ T_{\rm ant} &= \frac{S \ \eta \ A_g}{2 \ \pi \ \gamma_S^2 \ k_B} \ \int_{-\gamma_S}^{\gamma_S} e^{-(\log 2) \left(\frac{\alpha^2}{\alpha_w^2} \right)} \left[\int_{-\sqrt{\gamma_S^2 - \alpha^2}}^{\sqrt{\gamma_S^2 - \alpha^2}} e^{-(\log 2) \left(\frac{\beta^2}{\beta_w^2} \right)} \, d\beta \right] d\alpha \ . \end{aligned} \tag{17}$$

Since the Sun has been assumed to have a circular symmetry that $A(\alpha, \beta)$ lacks, this integral is non-trivial. There are two basic approaches to its evaluation. First, we use computer software to evaluate the integral numerically. Second, we make simplifying assumptions about the shape of the beam so as to evaluate the integral analytically.

1.4.1. Numerical Evaluation

Turning to Mathematica, we find that

$$T_{\rm ant} = \frac{S \ \eta \ A_g}{2 \ \pi \ \gamma_S^2 \ k_B} \left(5.96 \times 10^{-5} \right) \ . \tag{18}$$

Solving for the aperture efficiency η, we find

$$\begin{aligned} \eta &= \frac{2 \ k_B \ T_{\rm ant} \ \pi \ \gamma_S^2}{(5.96 \times 10^{-5}) S \ A_g} = \frac{(2) \left(1.38 \times 10^{-23} \, \frac{\rm J}{\rm K} \right) (313 \ {\rm K}) (\pi) (0.00436)^2}{(5.96 \times 10^{-5}) \left(5.4 \times 10^{-21} \ \frac{\rm J}{\rm m^2} \right) (4.11 \ {\rm m}^2)} \\ \eta &= 0.39 \ . \end{aligned} \tag{19}$$

1.4.2. Analytical Evaluation

The elliptical shape of $A(\alpha, \beta)$ is the primary source of our difficulties in directly evaluating the above expression for $T_{\rm ant}$. Thus far, we have treated the beam as being elliptical. However, since

the eccentricity of this ellipse is relatively small, we now make the simplifying assumption that it is circular. Subsequently,

$$T_{\rm ant} = \frac{S\ \eta\ A_g}{2\ \pi\ \gamma_S^2\ k_B}\ \int_{-\gamma_S}^{\gamma_S} \int_{-\sqrt{\gamma_S^2-\alpha^2}}^{\sqrt{\gamma_S^2-\alpha^2}} e^{-(\log 2)\left(\frac{\alpha^2+\beta^2}{\theta_w^2}\right)}\ d\beta\ d\alpha\ , \tag{20}$$

where

$$\theta_w = \frac{\alpha_w + \beta_w}{2} = 2.8^{\rm o} = 0.0489\ . \tag{21}$$

As the integrand is now completely circularly symmetric, we define

$$\begin{cases} \theta^2 = \alpha^2 + \beta^2 \\ \tan\phi = \beta/\alpha \end{cases}\ . \tag{22}$$

Therefore, $d\alpha\ d\beta = \theta\ d\theta\ d\phi$ and

$$\begin{array}{l} T_{\rm ant} = \frac{S\ \eta\ A_g}{2\ \pi\ \gamma_S^2\ k_B}\ \int_0^{2\pi}\int_0^{\gamma_S} e^{-(\log 2)\left(\frac{\theta^2}{\theta_w^2}\right)}\ \theta\ d\theta\ d\phi \\ T_{\rm ant} = \frac{S\ \eta\ A_g}{\gamma_S^2\ k_B}\ \int_0^{\gamma_S} e^{-(\log 2)\left(\frac{\theta^2}{\theta_w^2}\right)}\ \theta\ d\theta \end{array}\ , \tag{23}$$

We define $u = -(\log 2)\left(\theta^2/\theta_w^2\right)$ so that $du = -(\log 4)\left(\theta\ d\theta/\theta_w^2\right)$ and $\theta\ d\theta = -du\ \theta_w^2/(\log 4)$. Subsequently,

$$\begin{array}{l} T_{\rm ant} = \frac{S\ \eta\ A_g}{\gamma_S^2\ k_B}\ \frac{\theta_w^2}{\log 4}\ \int_{-(\log 2)\left(\gamma_S^2/\theta_w^2\right)}^{0} e^u\ du \\ T_{\rm ant} = \frac{S\ \eta\ A_g}{\gamma_S^2\ k_B}\ \frac{\theta_w^2}{\log 4}\ \left[1 - e^{-(\log 2)\left(\gamma_S^2/\theta_w^2\right)}\right] \\ T_{\rm ant} = \frac{S\ \eta\ A_g}{\gamma_S^2\ k_B}\ \frac{\theta_w^2}{\log 4}\ \left[1 - e^{-(\log 2)\left(\gamma_S^2/\theta_w^2\right)}\right] \end{array}\ . \tag{24}$$

Based on the above values, γ_S^2 is smaller than θ_w^2 by more than two orders of magnitude. Thus, we make the approximation that

$$\begin{array}{l} T_{\rm ant} = \frac{S\ \eta\ A_g}{\gamma_S^2\ k_B}\ \frac{\theta_w^2}{\log 4}\ \frac{\gamma_S^2\ \log 2}{\theta_w^2} \\ T_{\rm ant} = \frac{S\ \eta\ A_g}{2 k_B} \end{array}\ . \tag{25}$$

Note that in this limit (where the Sun is unresolved), the equation for $T_{\rm ant}$ reduces quite elegantly to an expression that is independent of both the angular size of the Sun and the beam-width. Solving for the aperture efficiency, we find that

$$\begin{array}{l} \eta = \frac{2\ k_B\ T_{\rm ant}}{S\ A_g} \\ \eta = \frac{(2)\left(1.38\times10^{-23}\ {\rm J/K}\right)(313\ {\rm K})}{(5.4\times10^{-21}\ {\rm J/m^2})\ (4.11\ {\rm m^2})} \\ \eta = 0.39 \end{array}\ . \tag{26}$$

It is very interesting to note that this is the same value to within our precision that we obtained for η using numerical methods to evaluate the integral over an "ellipsoidal" beam.

1.5. Expected Solar Flux Density

The flux-density of the (uniform, circular) Sun is

$$S_\nu = \Omega_S \; I_\nu = \pi \; \gamma_S^2 \; I_\nu \; , \tag{27}$$

where I_ν is the intensity of the Sun and $\Omega_S = \pi\gamma_S^2$ is the solid angle subtended by the Sun. Using the Rayleigh-Jeans approximation for I_ν gives

$$\begin{aligned} S_\nu &= \left(\frac{2\nu^2 k_B T}{c^2}\right)\left(\Omega_s^2\right) = \frac{(2)\left(1.38\times10^{-23}\ \frac{\mathrm{J}}{\mathrm{K}}\right)(5800\ \mathrm{K})\left(5.97\times10^{-5}\right)\nu^2}{\left(3.00\times10^{8}\ \frac{\mathrm{m}}{\mathrm{s}}\right)^2} \\ S_\nu &= \left(1.06\times10^{-40}\ \frac{\mathrm{J\ s^2}}{\mathrm{m^2}}\right)\left(\nu^2\right) \; , \end{aligned} \tag{28}$$

where we have adopted the optical brightness temperature of the Sun $T = 5800$ K. Evaluating this at $\nu = \nu_0 = 1.42 \times 10^9$ Hz gives

$$S_{\nu_0} = 2.14 \times 10^{-22} \; \frac{\mathrm{J}}{\mathrm{m^2}} = 2.14 \times 10^{-22} \; \frac{\mathrm{W}}{\mathrm{m^2\ Hz}} = 2.14 \times 10^4 \; \mathrm{Jy} \; . \tag{29}$$

Note that this is quite a bit less than the NOAA-observed value of $S_{\nu_0} = 5.4 \times 10^5$ Jy.

Recall that in this calculations, we treated the Sun as a uniformly bright disk with the Sun's optical radius and a brightness temperature of $T = 5800$ K. While both of these assumptions are valid for very short wavelengths, they do not apply at $\lambda_0 = 21$ cm (3). In fact, the effective radius of the Sun increases by about a factor of 1.2 and is significantly brighter around its edge than at its center (Figure 1). Additionally, the mean brightness temperature of the quiet Sun at $\lambda_0 = 21$ cm is about $T = 10^5$ K; during periods of intense stellar activity, this figure can increase by a factor of 100 (Figure 2). Taking these into account, a better estimate of the expected flux-density from the (quiet) Sun is

$$\begin{aligned} S_{\nu_0} &= \left(2.14\times10^{-22}\ \tfrac{\mathrm{J}}{\mathrm{m^2}}\right)(1.2)^2\left(\tfrac{10^5\ \mathrm{K}}{5800\ \mathrm{K}}\right) \\ S_{\nu_0} &= 5.3\times10^{-21}\ \tfrac{\mathrm{J}}{\mathrm{m^2}} = 5.3\times10^{-21}\ \tfrac{\mathrm{W}}{\mathrm{m^2\ Hz}} = 5.3\times10^5\ \mathrm{Jy} \; , \end{aligned} \tag{30}$$

which is much closer to the NOAA-observed value of $S_{\nu_0} = 5.4 \times 10^5$ Jy.

1.6. Galactic Rotation Curve

Based on the Galactic differential rotation model (Fig. 3), we can estimate the receding velocity of hydrogen clouds in the galactic plane for a given galactic longitude l. From the figure we see that the line of sight intersects the ring of rotational angular velocity $\Omega(R)$ twice. This can be seen also from using the cosine rule as shown in Fig. 4

$$R^2 = R_\odot^2 + D^2 - 2R_\odot \; D\cos l \tag{31}$$

where R is the galactocentric radius of the source, $R_\odot$ is the galactocentric radius of the Sun and D is the distance between both. The equation above is a quadratic equation for D with two solutions D_1 and D_2. These two distances form the triangle of sides $D_1, R, R_\odot$ and angles l, α and $(\pi - l - \alpha)$ and the triangle of sides $D_2, R, R_\odot$ and angles l, β and $(\pi - l - \beta)$ respectively according to Fig. 4. The angles l, α and β are related by the equality: $\cos(\beta + l) = \sin(\alpha + l)$.

Ignoring peculiar motions and based just on the assumption that the Galaxy undergoes differential rotation (i.e $v = v(R)$ or $\Omega = \Omega(R)$), we can write the receding velocity of HI gas in the Galactic disk relative to the Sun (the LSR) simply as

$$V_1 = v(R)\sin(l + \alpha) - V_\odot \sin l \quad (32)$$

$$V_2 = v(R)\cos(l + \beta - \pi/2) - V_\odot \sin l \quad (33)$$

where we have just projected each velocity onto the vector defined by the line of sight. Considering the relation between α and β, we obtain that $V_1 = V_2$, that is, the receding velocities from each point of the ring of velocity $v(R)$ are indistinguishable and contribute in the same form to the HI spectrum, unless precise distances can be provided. The situation in which this velocity contribution can be uniquely identified is in that one where the solution to D given l is unique. This happens at the tangent point of the circle or radius R given a line of sight l (see Fig 5). At this point,

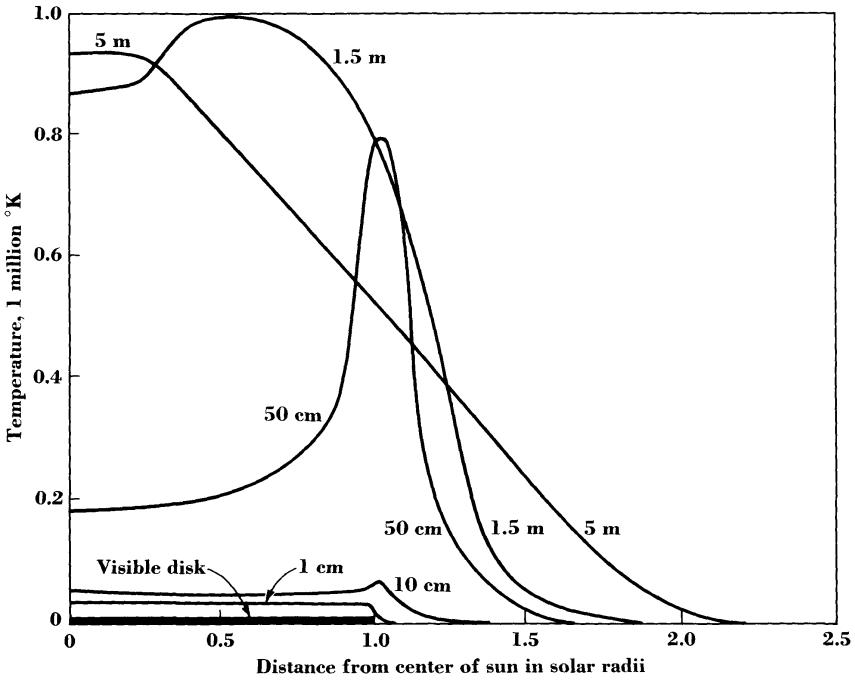

Fig. 1.— The brightness temperature of the Sun as a function of distance from the the center for select wavelengths [3].

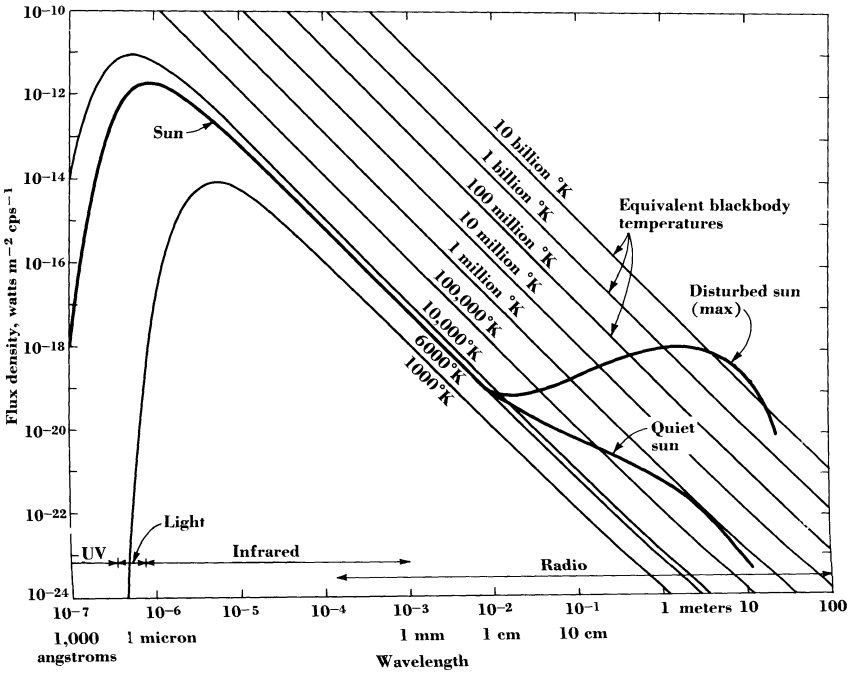

Fig. 2.— The mean brightness temperature of the Sun as a function of wavelength (thick curve) against black-bodies at various temperatures [3].

$\alpha + l = \pi/2$ hence the receding velocity is a maximum. Looking for a maximum velocity is equivalent to observing at the tangent point of a circular trajectory of radius R.

$$\begin{aligned} & \sin(l+\alpha) = \cos(l+\beta) = 1 \\ \Rightarrow \quad & V_1 = V_2 = V_{\max} = \upsilon(R) - V_\odot \sin l \end{aligned} \tag{34}$$

Furthermore, being this velocity associated to a single point, we can uniquely determine its distance. This means that, for the quadratic equation in D

$$D_{1,2} = R_\odot \cos l \pm \sqrt{R_\odot^2 \cos^2 l + R^2 - R_\odot^2} \tag{35}$$

we need that $D_1 = D_2$ i.e.,

$$\begin{aligned} & \sqrt{R_\odot^2 \cos^2 l + R^2 - R_\odot^2} = 0 \\ \Rightarrow \quad & 1 - \cos^2 l = \left(\frac{R}{R_\odot}\right)^2 \\ \Rightarrow \quad & \sin l = \frac{R}{R_\odot}. \end{aligned} \tag{36}$$

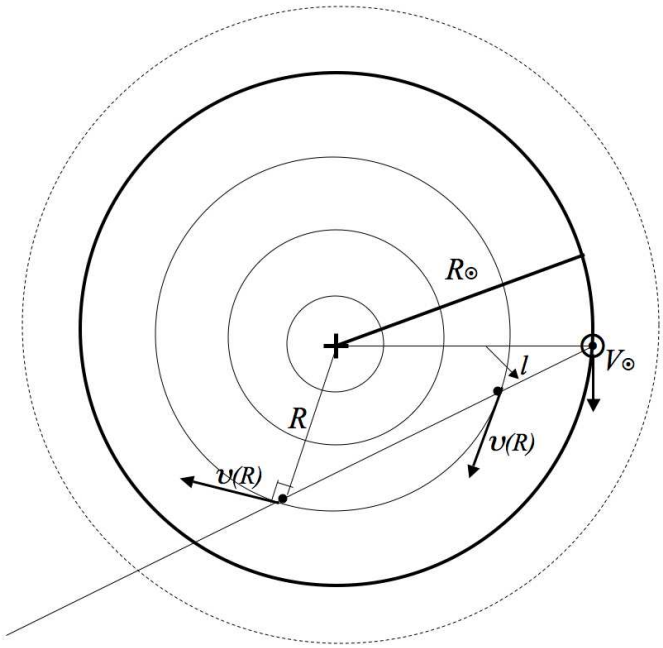

Fig. 3.— Galactic differential rotation. For each line of sight in the first and fourth quadrants in galactic coordinates (l, b) – i.e. the inner Galaxy – two points with the same linear velocity and the same distance from the Galactic Center are intercepted. Without auxiliary distance indicators, these two points are indistinguishable, introducing an ambiguity.

Hence, for galactocentric radii that satisfy $R = R_\odot \sin l$ – i.e. the line of sight grazes the smallest ring which it can get information from – the distances R, $R_\odot$ and D form a rectangle triangle as seen in Fig. 5 and the receding velocity observed coming from that point of the galactic plane is fully directed parallel the line of sight vector.

Unfortunately, Eq.31 does not have two solutions when $R > R_\odot$ (we would obtain a negative distance). This means that we cannot relate the maximum measured velocity to a given distance unless we know the distance to the source from an independent method (Fig. 6). For this reason, quadrant 3 and 4 in galactic coordinates are of no use in the determination of the rotation curve. Our data should be restricted to longitudes between 0° to 90° and from 270° to 360°. Nevertheless, we can derive a velocity equation valid in the second quadrant ($90° < l < 180°$). Indeed, in Fig. 6, we have that

$$V = v(R) \sin\beta - V_\odot \sin l = \Omega(R) R \sin\beta - \Omega(R_\odot) R_\odot \sin l.$$

But, using the law of sines,

$$\frac{\sin l}{R} = \frac{\sin\beta}{R_\odot}.$$

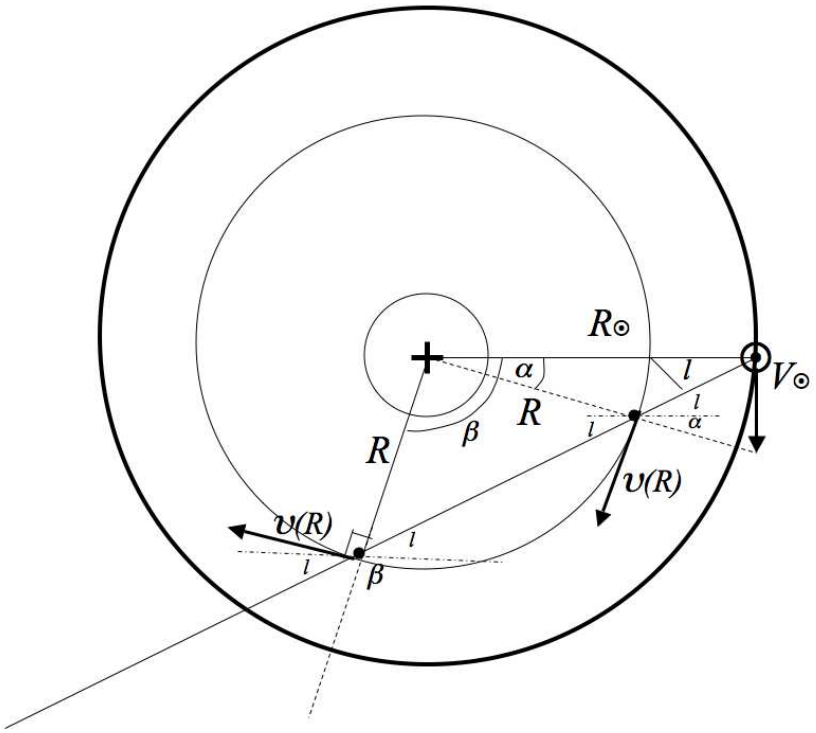

Fig. 4.— Geometry of the distance ambiguity. For a given line of sight – angle l – two points at different distances will be observed to have the same projected velocity.

Hence

$$V = \left(v(R)\frac{R_\odot}{R} - V_\odot \right) \sin l = \left(\Omega(R) - \Omega(R_\odot)\right) R_\odot \sin l. \tag{37}$$

which reduces to Eq. 34 when $\sin l = R/R_\odot$.

In a plausible rotational regime – in which $\Omega(R) \leq \Omega(R_\odot)$ for $R > R_\odot$ – since for the second quadrant $\sin l > 0$, we would expect negative radial velocities in this quarter of the Galactic plane. Using the same reasoning, we should expect only positive radial velocities in the third quadrant ($180° < l < 270°$), since for this region, $\sin l < 0$. However, this is a fragile assumption, since different galaxies show a rotation curve that flattens at intermediate radii without decaying in a keplerian form, as it could be expected. But even under these circumstances, we will expect very small or negative velocities as long as the $R > R_\odot$ condition is fulfilled. But unless we know R (or D) we can't assign directly the measured velocity to a distance from the Galactic center. This is why clusters, stars or other standard candles are used to construct the rotation curve of the outer milky way, instead of neutral hydrogen. Neutral hydrogen can be used in more sophisticated analysis, with observations covering the thickness of the galactic disk and assuming a scale height/galactocentri distance relation.

1.6.1. The Data

In two opportunities, HI spectra were taken using the Haystack satellite dish (Tables 2 and 3). The beam was pointed to the Galactic plane ($b \approx 0°$) and measurements at different longitudes were taken. Based on the arguments above, for each longitude l, the maximum velocity (maximum redshift of the HI 21 cm line) for which emission was detected was identified as $V_{\rm max}$. One of the uncertainties in this method was the evident existence of a spectral linear baseline which we did not have time to estimate an subtract from each spectrum. In addition, the random motions of the gas impose a limit in the accuracy with which the bulk orbital velocity can be measured. The results are listed below.

Following the expressions below (from Eqs. 36 and 34), we can compute the galactocentric radius R and the linear rotational velocity $v(R)$

$$R = R_\odot \sin l \tag{38}$$

$$v(R) = V_{\rm max} + v_\odot \sin l \tag{39}$$

where the values of $v_\odot = 220$km s^{-1} and $R_\odot = 8.5$ kpc were used to calculate the Galactic rotation curve.

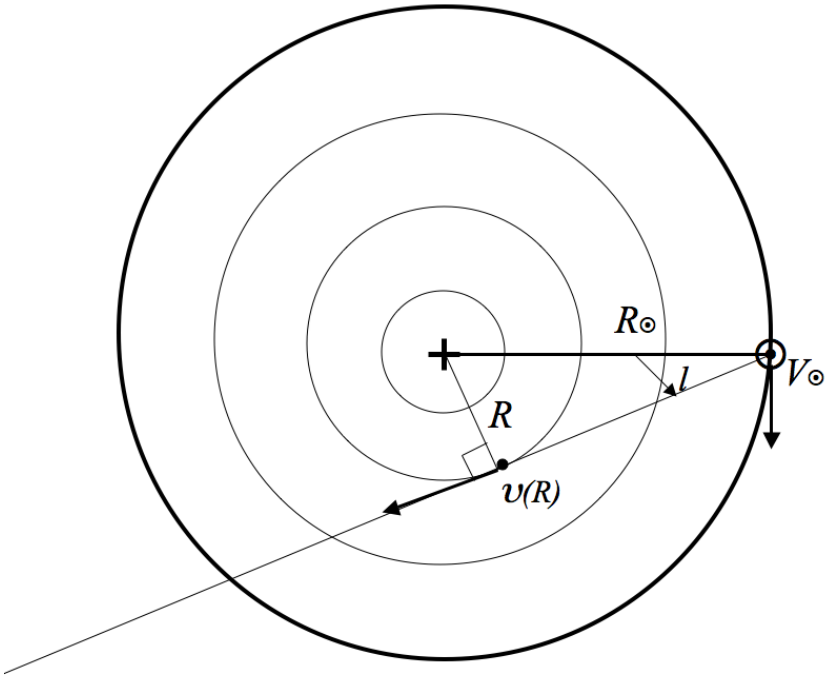

Fig. 5.— Line of sight reaching tangentially the ring of radius R.

Table 2: Ben and Diego's Galactic Rotation Curve Data

l	$V_{\max}$	$V_{\max} + v_{\odot} \sin l$ [km s^{-1}]	$R_{\odot} \sin l$ [kpc]
0	30	30	0
8	50	80.6	1.2
14	70	123.2	2.1
30	120	230.0	4.3
49	80	246.0	6.4
60	55	245.526	7.4
95	20	239.163	8.5
110	15	221.732	8.0

Table 3: Robert and Claude-Andre's Galactic Rotation CurveData

l	$V_{\max}$	$V_{\max} + v_{\odot} \sin l$ [km s^{-1}]	$R_{\odot} \sin l$ [kpc]
0	30	30	0.0
10	55	93.2	1.5
14	80	133.2	2.1
30	120	230.0	4.3
37	110	242.4	5.1
49	90	256.0	6.4
59	60	248.6	7.3
67	50	252.5	7.8
81	30	247.3	8.4
88	20	239.9	8.5
99	10	227.3	8.4
117	5	201.0	7.6
132	5	168.5	6.3

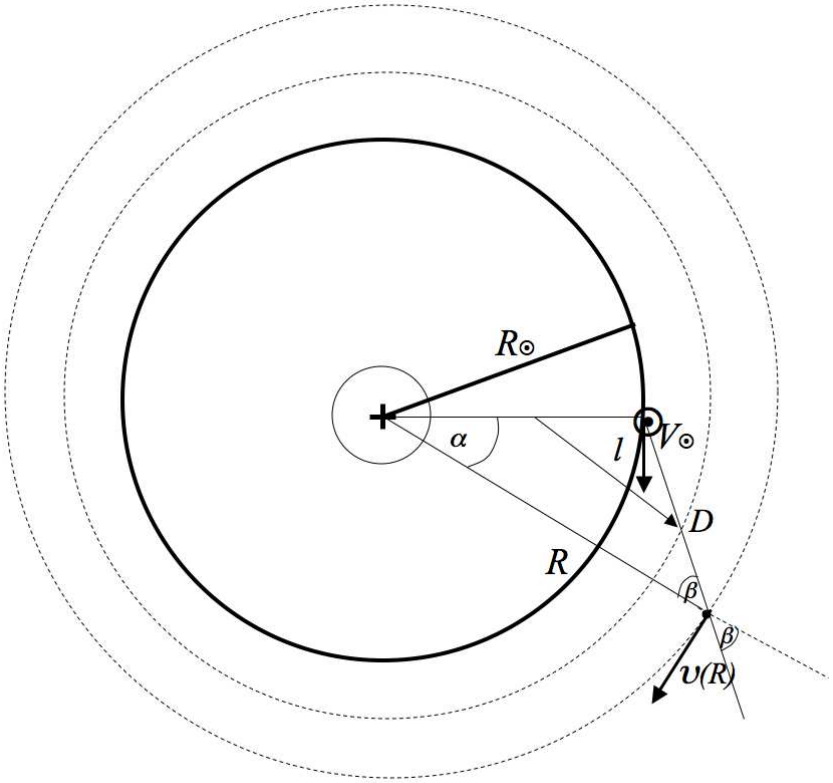

Fig. 6.— Observing in the Galactic second quadrant.

We have constructed rotation curves in Figs. 7 and 8 from data sets in Tables 2 and 3. We have excluded data points in the second quadrant and we attribute positive velocity measurements to random motions deviating from the circular rotation assumption. These measurement are very close to $l = 90^\circ$ longitude for which we expect $V \approx 0$ (see Eqs. 36 and 34) since we do not expect non-zero motions for gas in the solar circle respect to the LSR. In that case, measurements of $V_{\rm max} \approx 5 - 10$ km s^{-1} are exclusively due to random motions. Thus, an error of ± 10 km s^{-1} is intrinsic to every measurement.

Figures 7 and 8 show a rotation curve that flattens at a radius of ~ 4 kpc. The quantities in the plot are strongly dependent on the values of $R_\odot$ and $v_\odot$, the qualitative shape of the rotation curve, however, remains unaltered if these values are varied.

2. Haystack Project 2: Angular Size of the Sun (led by Sarah Ballard)

We first need to establish which observations are useable. Due to cloud cover, we cannot use data taken below an elevation angle of about 10°. The bandwidth estimate of 60 MHz may also be slightly incorrect; at times relatively far from where the delay was set to zero (18.5 hours), this effect is large and makes the data untrustworthy. These constraints leave about 30 good observations.

2.1. Calculating the projected baseline length

The angle ψ between the baseline vector and the unit vector in the direction of the source, in local coordinates, is given by Equation 40. E_B is the elevation angle of the baseline and AZ_B is the azimuth angle of the baseline (0° and 82° for our observations, respectively).

$$\cos(\psi) = \sin(E_B)\sin(E_S) + \cos(E_B)\cos(E_S)\cos(AZ_S - AZ_B) \tag{1}$$

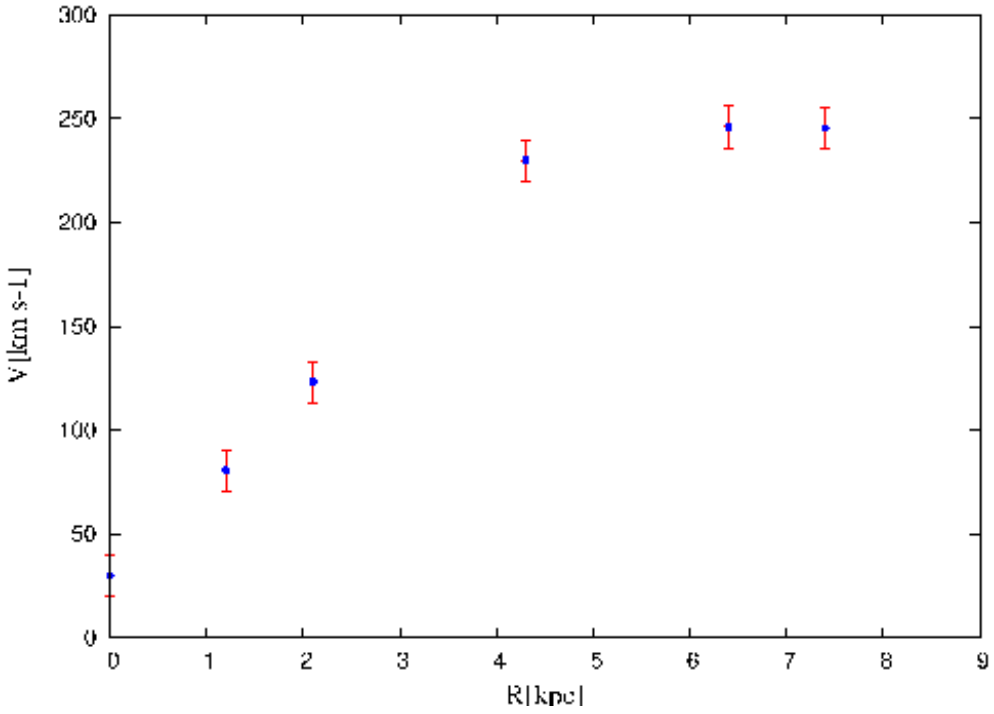

Fig. 7.— Rotation curve from Table 2 excluding observations beyond a longitude of 90°.

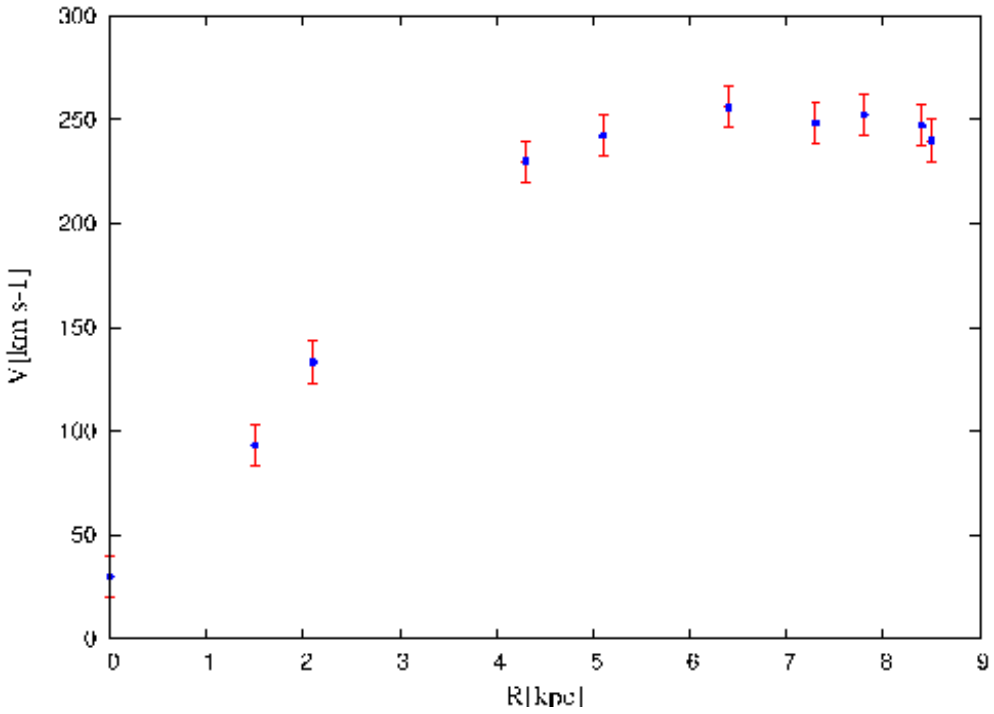

Fig. 8.— Rotation curve from Table 3 excluding observations beyond a longitude of 90°

We can convert the measured elevation and azimuth angles of the sun, E_S and AZ_S, to projected baselines by the relationship $D_{proj} = D \sin\psi$. Fig. 2.1 gives a plot of projected baseline as a function of UT time for the observations that were useable. The kink in D_{proj} at a UT of around 19 is due to an offset in ψ that occurred when the telescope was repointed mid-observation.

2.2. The effect of the finite bandwidth on the fringe visibility

We know from lecture that the additional path length for light between the two antennas will result in a sinc contribution to the visibility, of the following form, where V_{uncor} is the visibility function with no delay compensation (as was the case for this experiment), V is the actual visibility function, $\Delta\omega$ is the bandwidth ($2\pi\Delta\nu$, where $\Delta\nu$ is 60 MHz, the given filter width), and $D\cos\psi$ is the propagation path difference for a given observation. We know that Dr. Rogers turned the delay compensation to be zero at UT=18.5 hours, so the $\cos\psi$ at that time needs to be subtracted from the argument, in order to make the delay function equal to one at 18.5 hours.

$$V_{uncor} = V\frac{\sin(D(\cos\psi - cos\psi_{18.5})\Delta\omega/2c)}{D(\cos\psi - \cos\psi_{18.5})\Delta\omega/2c} \tag{2}$$

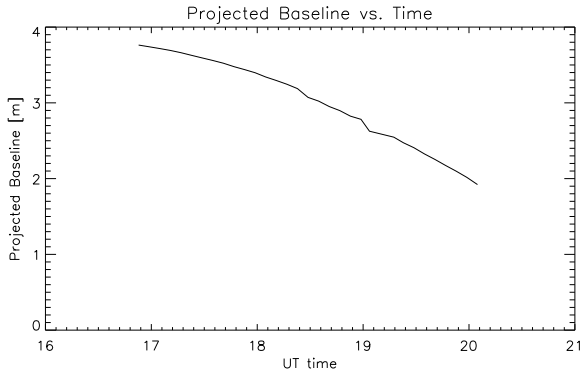

Fig. 9.— Projected baseline versus time, for useable observations.

Alternatively, instead of multiplying the model visibility function by this delay function, we can divide the measured visibility by the delay. We took this approach, so the visibility function model would be simpler.

2.3. Fitting to the function of a uniformly bright disk

As derived in lecture, the visibility function for a given intensity $I(\theta)$ is given by the following, where J_0 is the zeroth order Bessel function, and q is the baseline distance D divided by λ.

$$V(q) = 2\pi \int_0^{\theta} I(\theta) J_0(2\pi q\theta)\theta \, d\theta \tag{3}$$

For $I(\theta)$ constant to some θ_C and zero elsewhere (that is, a uniformly bright disk), then the visibility is given by Equation 43, where J_1 is the first order Bessel function and I_D is the intensity of the disk.

$$V(q) = 2\pi I_D \theta_C^2 \frac{J_1(2\pi q\theta_C)}{(2\pi q\theta_C)} \tag{4}$$

We can verify this visibility by using the fact that $V(q = 0)$ should equal the total flux. Evaluating this $V(q)$ at 0, we find that it is indeed equal to $I_D \pi \theta_C^2$, the expected flux from a disk of intensity I_D and solid angle $\pi\theta_C^2$.

After dividing the measured visibility V_{uncor} by the sinc delay, as in Equation 2, we can compare

the expected visibility function V with what was observed. By solving for the best-fit θ_C, we can measure the angular radius of the sun. We carried out a simplified χ^2 analysis to find the best-fit θ_C, where χ^2 is defined below:

$$\chi^2 = \sum_{i=1}^{N} \frac{(model_i - data_i)^2}{\sigma_i^2} \tag{5}$$

Here $model_i$ is the best guess for the visibility function at a given point, and $data_i$ is the actual data at that point. While we do have the errors associated with each observation, for this fit we elected just to set $\sigma_i = 1$ at all points. Since the errors are less than a percent of the data, they probably do not represent the true error. This may be due to systematic errors in receiver gain drift or pointing. We fit for two degrees of freedom: the angular radius of the sun θ_C, and the amplitude a of the J_1 Bessel function, so that the model was given by Equation 6, where we have replaced q by D_{proj}/λ. Fitting for the amplitude was necessary because the measured visibility function is not normalized to peak at one.

$$model_i = a \mid \frac{J_1(2\pi D_i \theta_C/\lambda)}{(2\pi D_i \theta_C/\lambda)} \mid \tag{6}$$

Because the measured visibility is only positive, we took the absolute value of the model visibility.

Then we searched the χ^2 space for the θ_C and a for which the χ^2 was minimized. We found the best-fit θ_C to be 16.58 $\pm$ 0.01 arcminutes, and the best-fit a to be 586 $\pm$ 2. The best-fit visibility function, with data overplotted, is shown in Fig. 10.

The total optical angular size of the sun on Nov. 9, 2007 was 32.3'. From Fig. 1, the radius of the sun at 1 cm wavelength is about 1.05 times the optical radius of 16.15', and the radius of the sun at 10 cm is about 1.4 times the optical radius. At around 2.5 cm (the wavelength at 12 GHz), we might expect a radius of around 1.05 times the optical radius of the sun, or 16.95'. Our measured radius of 16.58', about 1.03 times the optical radius, is fairly close to this value.

2.4. Effects of limb brightening

To create a model visibility function that includes limb brightening, we can assume an intensity function which behaves as a constant out to some θ_C, and add to it a delta function ring at θ_C of some brightness I_R. Plugging this model intensity into Equation 42, we obtain the visibility function given by Equation 46. Here we have defined I_R to be the intensity of the ring, which has

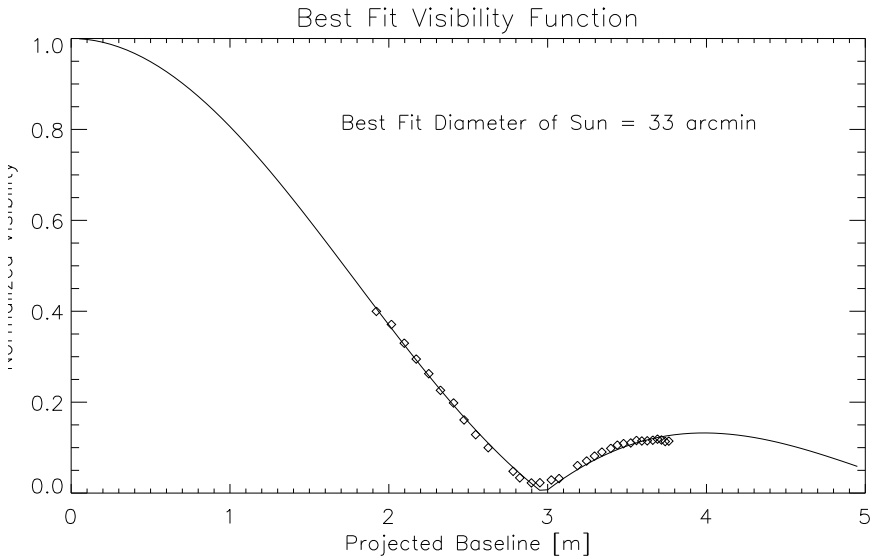

Fig. 10.— The best fit visibility function with data overplotted. The best fit angular size of the sun was measured to be 33.2', about 3% larger than the optical angular size of 32.3'.

some thickness θ_R starting at θ_C, the radius of the sun (although I have evaluated the visibility of the ring as though it were a delta function at θ_C, in reality the ring will have a finite thickness). We see again that this $V(q=0)$ is equal to the sum of the fluxes from the disk and the ring, as it should be (note that $J_1(x)/x$ evaluated at zero is 0.5, and $J_0(x)$ evaluated at zero is 1).

$$V(q) = 2\pi I_D \theta_C^2 \frac{J_1(2\pi q\theta_C)}{(2\pi q\theta_C)} + 2\pi I_R \theta_C \theta_R J_0(2\pi q\theta_C) \tag{7}$$

We can normalize this visibility by defining a parameter f, the ratio of the fluxes from the ring and the disk, given by Equation 47. Then the normalized visibility is given by Equation 48.

$$f = \frac{F_{ring}}{F_{disk}} = \frac{2\pi I_R \theta_C \theta_R}{\pi I_D \theta_C^2} \tag{8}$$

$$V(q) = \frac{2J_1(2\pi q\theta_C)/(2\pi q\theta_C) + fJ_0(2\pi q\theta_C)}{1+f} \tag{9}$$

Just to visualize how the limb brightening term behaves in comparison with the standard visibility function, we have overplotted it in Fig. 11 for a fraction f of 25% (very high, just so it appears clearly on the plot). From this plot, it's clear that a contribution from limb brightening may account

for the fact that the null of the measured visibility function never goes completely to zero. Although our measurement errors are not reliable enough to perform a meaningful χ^2 analysis to test the limb brightening hypothesis, we can at least set an upper bound on the limb brightening fraction f. A larger f than this value would result in a higher null than observed. Fig. 12 shows an inset of the original best-fit visibility to the data, with an approximate limb brightening contribution overplotted at an f of 5%. A fraction much higher would clearly be inconsistent with the two lowest observations.

We can compare this result to Fig. 1 to check its validity. Equation 47 reduces to Equation 49 for r defined to be the thickness of the ring as a fraction of solar radius.

$$f = \frac{2rI_R}{I_D} \tag{10}$$

Fig. 1 is defined in terms of brightness temperature, which is linearly related to intensity, so we can directly compare a ratio in I to ratios in temperature inferred from the figure. For 10 cm observations in Fig. 1, the temperature as a function of radius shows a slight peak, at total radius of the sun, of about 110% the temperature in the disk. This peak is spread over a width of about 5% the radius of the sun. From Equation 49, we would then expect a limb brightening fraction f of around 11% or so at 10 cm. However, at 1 cm, the figure shows almost no evidence of limb brightening. An upper limit of about 5% is therefore reasonable for observations at the intermediate wavelength of 2.5 cm.

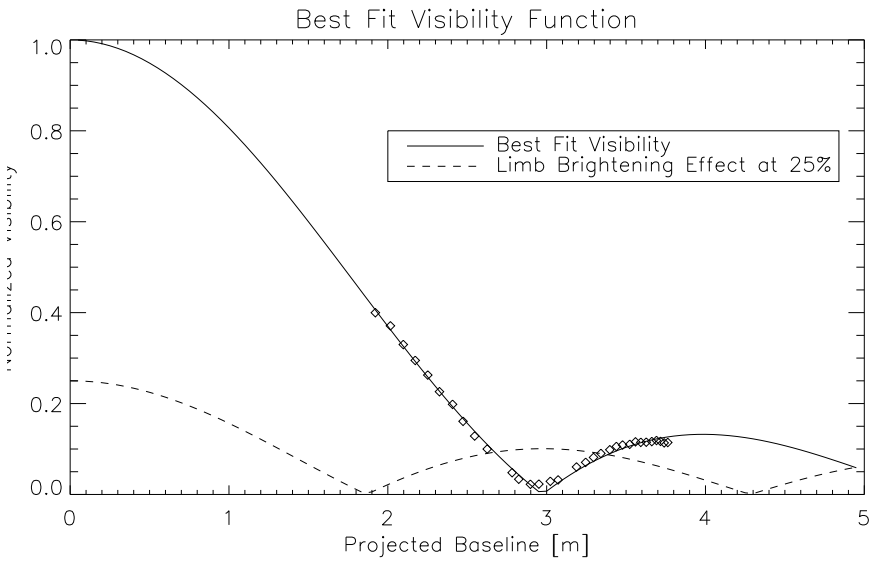

Fig. 11.— The bestfit visibility function with the extra limb brightening term (at a fraction of 25% of the disk intensity), just to compare their behaviors.

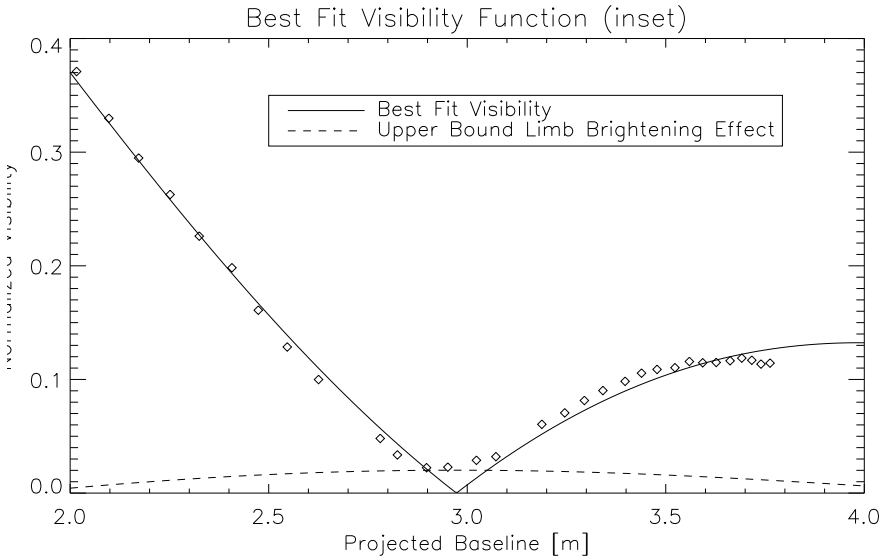

Fig. 12.— Inset of best-fit visibility function, with maximum limb brightening contribution (at 5%) overplotted. It's clear that a limb brightening fraction any higher would be inconsistent with the observations.

2.5. Fitting parameters vs. inverse Hankel transform

An alternative to fitting model parameters to the data might be directly taking the inverse Fourier transform of the measured visibility (actually a Hankel transform here, since the source is assumed to be spherically symmetric). However, this alternative is not feasible due to the finite extent (in baseline space) of our data. Taking the inverse Fourier transform of only a known piece of the visibility function will return something unrecognizable. Even if the observed visibility was a perfect "Jinc" function over some finite range in baseline space (where "Jinc" is $J_1(x)/x$), the resulting inverse Hankel transform would have a "ringing" effect of sidelobes.

3. Haystack Project 3: Measurements of the Visibility of a Single and Double Source (led by Robert Harris and Lauranne Lanz)

In this project, our goal was to measure the response of a two-element interferometer to a pair of fluorescent light bulbs that emitted predominantly at $\nu = 12$ GHz. Below, we describe the basic theory behind this project, present the setup and procedures, and then give an analysis of the data.

3.1. Theory of Two-Element Interferometry

Assume that one is observing two point-like sources on the sky with a two- element interferometer. For concreteness, this situation is illustrated in Fig. 13. Assume that the double source consists of two delta functions of intensity, located at (α_0, β_0) and at $(-\alpha_0, -\beta_0)$ in the sky plane such that the angle the line connecting the two sources makes an angle θ with the α-axis. So, the intensity is given by:

$$I(\alpha, \beta) = I_0(\delta(\alpha - \alpha_0, \beta - \beta_0) + R\delta(\alpha + \alpha_0, \beta + \beta_0))$$

where R is the ratio of the intensities of the two sources. The visibility function is then just given by the integral of the intensity over the sky:

$$\begin{aligned} V(u,v) &= \int_{\text{sky}} I(\alpha,\beta)\exp[2\pi i(u\alpha + v\beta)]d\alpha d\beta \\ &= I_0(\exp[2\pi i(u\alpha_0 + v\beta_0)] + R\exp[-2\pi i(u\alpha_0 + v\beta_0)]) \\ &= I_0(\exp[\pi i\Delta\phi(u\cos(\theta) + v\sin(\theta))] + R\exp[-\pi\Delta\phi i(u\cos(\theta) + v\sin(\theta))]) \\ &= I_0\exp[\pi i\Delta\phi(u\cos(\theta) + v\sin(\theta))](1 + R\exp[-2\pi\Delta\phi i(u\cos(\theta) + v\sin(\theta))]) \end{aligned}$$

where $\Delta\phi$ is the angular extent of the double source (i.e. b/c) and α and β have been expressed in terms of θ and the angular extent of the source. It is clear that this will never be zero unless $R = 1$. Therefore, we fix $R = 1$, and compute $|V(u,v)|^2 = V^\dagger V$.

$$|V(u,v)|^2 = I_0^2(1 + R^2 + 2R\cos(2\pi\Delta\phi(u\cos(\theta) + v\sin(\theta))))$$

It is clear that this expression is zero when the argument of the cosine is an odd multiple of π. So, to compute the first null, we take:

$$\begin{aligned} 2\pi\Delta\phi(u\cos(\theta) + v\sin(\theta))) &= \pi \\ \rightarrow \Psi &= \frac{1}{2\Delta\phi} \\ \Psi &= \frac{c}{2b} \end{aligned}$$

where Ψ is defined to be $u\cos(\theta) + v\sin(\theta)$. Taking $\theta = 0$ (the double source aligned along the α-axis in the sky), we find that the first null occurs at $u = \frac{c}{2b} \rightarrow x = \frac{\lambda c}{2b}$. So, the separation for first null is given by

$$\Delta D = \frac{\lambda c}{2b}$$

Because approximating the fluorescent light bulbs in this experiment as point sources may not be a good approximation, we must also consider other possible shapes the lights might be considered to be when viewed from the interferometer. The two most likely to be good models for the distribution

of brightness for a single light bulb are the uniform disk and the uniform annulus. Fortunately, because the brightness distribution of two uniform disks (or annuli) at a separation b is just given by the convolution of the brightness of a uniform disk (or annulus) at the origin with the brightness distribution of the pair of delta functions, as outlined above, the visibility of two uniform disks or annuli is just given by the product of that of the pair of delta-functions with that of a single uniform disk or annulus.

For a uniform disk with angular radius R, the visibility function takes the form

$$V(u) = \frac{2J_1(2\pi uR)}{2\pi uR}.$$

For a thick annulus (one for which ΔR, the annulus thickness, is not much less than R), the inner radius, one must numerically integrate to obtain

$$V(u) = \frac{1}{R^2}\int_{R-\Delta R}^{R} 2rJ_0(2\pi ur)dr$$

Note that this converges to the visibility of the uniform disk in the limit $\Delta R \to 0$.

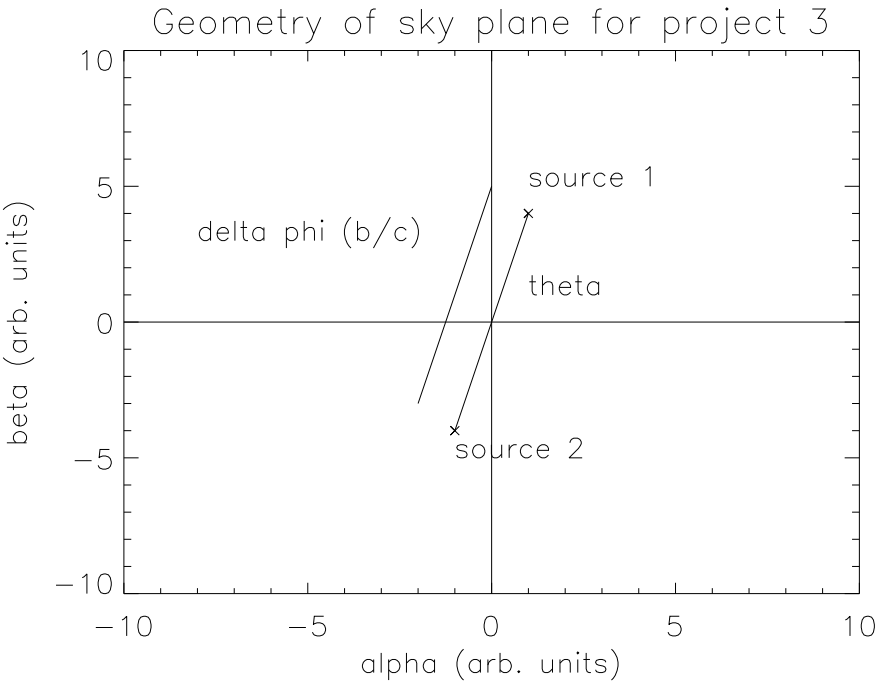

Fig. 13.— Illustration of the plane of the sky when observing a double source.

3.2. Experimental Setup and Procedures

To carry out our measurement of the visibility function, we used the setup shown in Fig. 14 that was provided to us by the staff at the Haystack observatory.

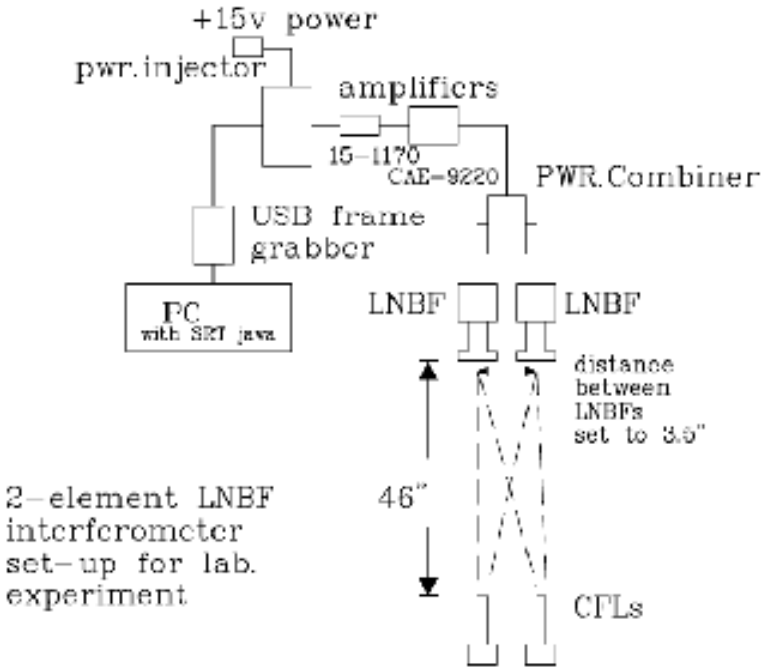

Fig. 14.— Circuit diagram for project 3. Obtained from VSRT Memo 025.

We note that although figure marks the distance between the feeds and the lamps to be 46 inches, our experiment had a different value, approximately 52 inches. Also, given that there were three feeds on each of the LNBF, we determined which was the active feed by blocking each in turn and seeing whether the values measured by the computer program when the lights were on changed.

The active feeds, hereafter referred to as the receivers, were placed side by side.

This experiment had three phases. For each phase, the distance between the receivers and the lamps was obtained. For each data point within a phase, information regarding the distance between the lamp centers, the distance between the receiver centers and the temperature value outputted by the computer program were recorded.

In phase 1, we measured the visibility function for a single fluorescent light. One of the two lamps was turned off and placed at a distance of 52.5 inches from the receivers. Its inner and outer radii were measured. Measurements of receiver separation and temperature from the computer program were recorded for twelve different receiver separations.

In phase 2, we measured the visibility function for the double fluorescent light source. The receivers were placed 52.5 inches from the lamps. The lamps were separated by 4.125 inches. The receivers were separated an increasing amount. At each step, the separation between the receiver centers and the temperature given by the computer program were recorded. The receiver to be moved was alternated. Further, as the separation became larger, the receivers were also tilted a bit towards the lamps so that the sources would still be within the beam. Twenty-one data points were taken.

In phase 3, we repeated the measurement performed in phase two, but by an alternate method. The receivers were placed 52.25 inches from the lamps and separated by 3 inches. The lamps, rather than the receivers, were then separated an increasing amount. At each step, the separation between the lamp centers was measured and the temperature given by the program was recorded. Twenty-five data points were taken.

After the data were taken for all three phases and analyzed, it was realized that there was a zero-point visibility that corresponded to noise-floor or bias for the interferometer. All data have been corrected for this by subtraction of the noise-floor from the measured visibilities, i.e. $V^2_{\rm corr} = V^2_{\rm measured} - B^2$ where $B = 12.7$ K.

3.3. Data and Analysis

3.3.1. Measurement of Single Source Visibility

The uncalibrated power (measured in Kelvin) detected for a single fluorescent light bulb was recorded as a function of the baseline separation between the two feeds. The distance between the bulb and the center of the baseline between the feeds was $52.5 \pm 1/16$ inches. The outer radius of the bulb was 1.31 inches and the inner radius was 1.0 inches.

Modelling the source as a uniformly bright disk, we fit the data for the single source visibility to the following form:

$$V_{\rm best-fit}(d) = a \left| \frac{J_1(bd)}{bd} \right| \tag{1}$$

where d is the length of the interferometer baseline, $a = 124.2 \pm 1.7$ K, $b = 0.184 \pm 0.004$ in^{-1}, where the errors on the best-fit parameters are 1-σ errors. This corresponds to a frequency of $\nu = 13.95 \pm 0.28$ GHz using the formula $0.609/\Delta\phi = x_0\nu/(bc)$, where $\Delta\phi$ is the angular extent of the source, b is the fit parameter above, and x_0 is the location of the first null. However, it is of note that the lightbulb resembled more closely a square lit at the edges than a uniformly illuminated circle. Therefore, approximating the fluorescent bulb as a square instead of a circle, the correct formula to use is $0.5/\Delta\phi = x_0\nu/(bc)$, which gives an estimate of the frequency at 11.46 ± 0.23 GHz. It is of note that both results are roughly consistent with the nominal frequency of the light, i.e. 12.0 GHz. However, the reduced χ^2 statistic for this fit was 15.01 with 10 degrees of freedom, which is a formally unacceptable result.

Due to the large χ^2 statistic for our model, we examined the residuals, defined as the deviation away from the fit expressed in terms of the error on each point. In fact, in Fig. 15(b), one observes a somewhat sinusoidal variation in the residuals of the fit, throwing some doubt onto our fit. One possible origin for the sinusoidal variations in the residuals is a relatively weak double source that is being detected by the feeds. It is possible that twin fluorescent lights on the ceiling could be the cause of this anomalous result. If the lights were at a large angle from the symmetry axis of the interferometer, then the gains of the feeds at that angle are expected to be small. Therefore, the lights might cause a small amplitude ripple in the visibility function. One might hope to be able to test this; however, this would require two additional parameters in the fit: that for the amplitude of the visibility fluctuation, and the product of the angular size of the source and the wavenumber of the radiation emitted from the fluorescent lights. Since we do not know the wavenumber of the extra sources with any accuracy, we cannot get a constraint on the angular size of the source, thus limiting our ability to confirm the hypothesis that ceiling lights are responsible for this effect.

To further explore the possible sources of large deviations away from the predicted visibility amplitude, we explored the possibility that the source might not be well-modelled by a uniformly bright circle or a square, but rather a circular annulus. We attempted to see if the source could be more accurately described by a circular annulus by performing the numerical integration mentioned in the previous subsection for the single source. We found that the sidelobes for the source should have been approximately 40% for a uniformly bright annulus. Our sidelobes are quite a bit lower than 40%, so it seems as though the ring description is less than optimal for our data.

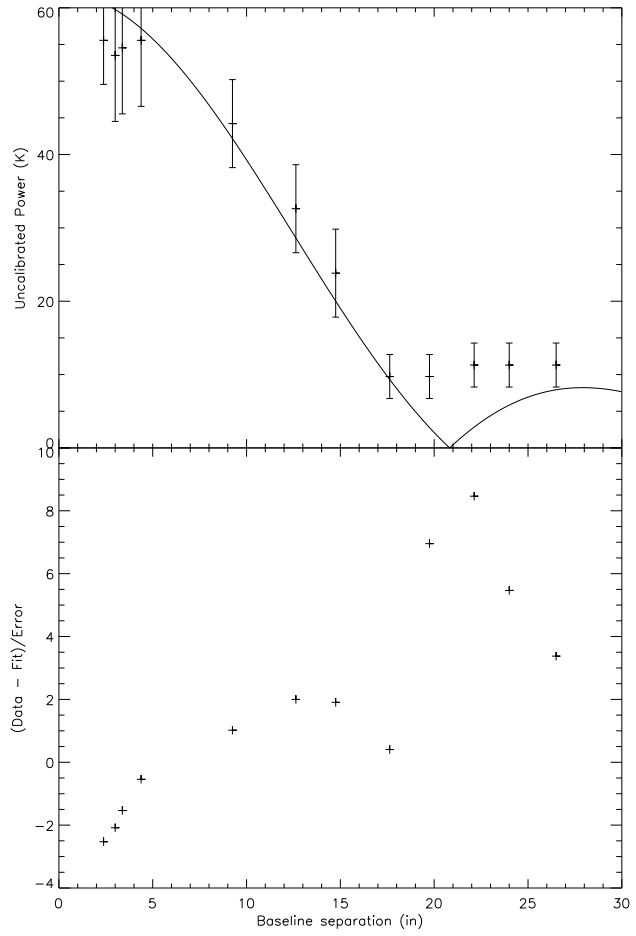

Fig. 15.— Measured and fit visibilities for a single fluorescent lamp. The top plot, (a), gives the measured (crosses with errors) and fit (solid line) power expressed in Kelvin as a function of baseline separation. The bottom plot, (b), gives the residuals of the fit expressed in terms of the estimated error on the measurements.

3.3.2. Measuring the Visibility as a Function of Baseline Separation

Having obtained an estimate of the center frequency of the inpinging radiation, we now turn to the second phase of our project, the measurement of the visibility function of the double source as a function of the baseline distance of the receivers. In this part of the experiment, we kept the separation of the two sources constant at 4.13 inches and the distance of the center of the baseline to the sources was kept at 52.5 inches, but we incremented the baseline by moving the detectors apart. We fitted the data to cosine term, modulated by a first order Bessel function divided by its argument (the so-called "jinc" function). The data, fit, and residuals are shown in Figure 16.

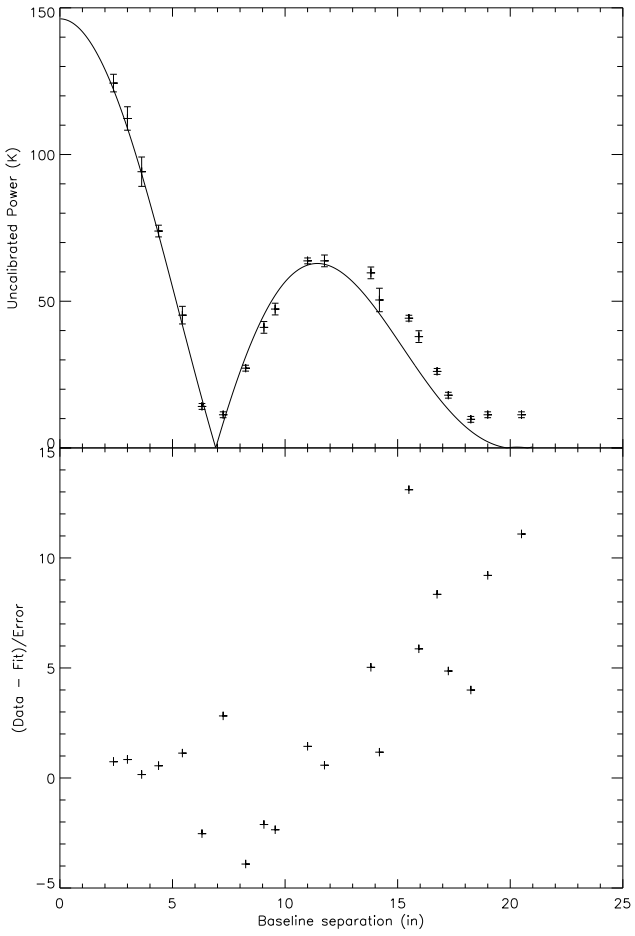

Fig. 16.— The top plot, (a), gives the measured (crosses with error bars) and fit (solid line) uncalibrated powers for a double source as a function of baseline separation. The bottom plot, (b), gives the residuals of the fit expressed.

The fit has the functional form

$$V(d) = \left| A\cos(Bd)\frac{J_1(Cd)}{Cd} \right|, \tag{2}$$

where d is the baseline separation and where the best-fit parameters are $A = 292.5 \pm 4.0$, $B = 0.227 \pm 0.002$, and $C = 0.193 \pm 0.005$.

Repeating the analysis performed in the first part of the project, we find the best-fit frequencies derived from the argument of the jinc function to be given by 12.78 ± 0.35 GHz. From the argument of the cosine, we can check the measurement of the wavelength of the light from the fluorescent sources. The first nulls of the cosine occur at arguments of $\pi/2$ and $3pi/2$, which, given first-nulls of 6.92 ± 0.05 in and 20.76 ± 0.14 in, both yield a frequency of 10.85 ± 0.11 GHz. We note that,

while the result from the argument of the jinc function is formally consistent with both the quoted frequency of the emitted light and the estimate of it from the visibility measurements of the single source, the results from the argument of the cosine in this measurement are only roughly consistent with them. The χ^2 statistic for this fit was formally unacceptable, with a reduced χ^2 of 1.82 for 18 degrees of freedom.

One possible clue for this quite remarkable inconsistency derives from the geometry of the setup. The light bulbs' length was substantially more than their radius. Therefore, the solid angle subtended by the lights at the distance of the receivers increased as the baseline increased, the limiting case of infinite separation corresponding to the entire emitting length of the bulb being visible. Since the residuals on the fit after a certain baseline separation are all positive (and large), it is probable that the changing aspect of the light with respect to the receivers played a large role in degrading the quality of the data. An possible improvement to the experimental setup would be to add a cover for the side of the lights so that changing the angle to the light source does not significantly alter the total amount of light received at the detector.

3.3.3. Measuring the Visibility as a Function of Source Separation

In the final phase of the project, we measured the effect of changing the source separation on the response of the receivers. For this, we used a distance from the center of the baseline to the sources of 52.5 inches with a baseline of 3 in. The data from these measurements are presented in Figure 17, in which we show the data along with a fit to a cosine term, representing the visibility of two sources that are moving as apart while the baseline of the interferometer is fixed, along with their residuals. Note the absence of a jinc modulation because the baseline is fixed.

The best-fit visibility as a function of source separation is given by

$$V_{\rm best-fit}(s) = A\,|\cos(Bs)|\,, \tag{3}$$

where the best fit parameters are given by $A = 142.2 \pm 5.9$ K, and $B = 0.175 \pm 0.002$ in^{-1}. For this value of B, the corresponding best-fit frequency is given by 11.62 ± 0.17 GHz, which is barely consistent with, the quoted value of ~ 12 GHz. The quality of the fit is, again, formally unacceptable, with a reduced χ^2 statistic of 2.11 with 22 degrees of freedom.

3.4. Discussion of Results

As we see in the previous subsection, the results for the determination of the visibility function of the double light source seem to match that which is expected from theory. The visibility of a double

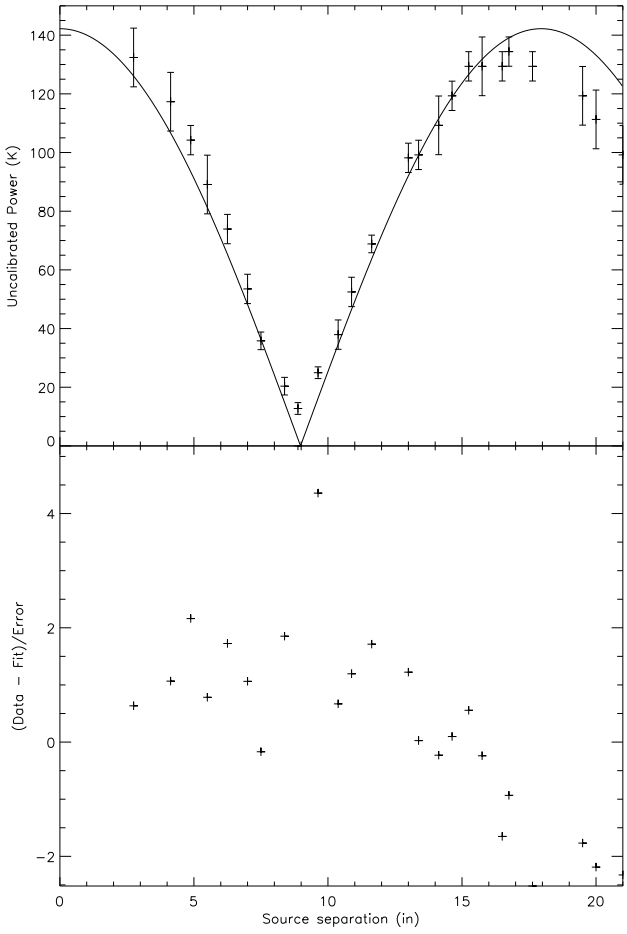

Fig. 17.— Measurement of the visibility of the double source as a function of source separation. The top plot, (a), gives the measured (crosses and error bars) and fit (straight line) uncalibrated powers for a double source as a function of source separation. The bottom plot, (b), gives the residuals of the fit.

source is expected to vary as the cosine of the angle between the sources and as $J_1(x)/x$ where x is a (dimensionless) baseline separation. Also, this latter dependence has been confirmed for the single source visibility as well. One may notice that our determination of the characteristic noise temperature in the system (the uncalibrated power with no light impinging on the interferometer) is remarkably constant at about 13 K.

However, problems remain. The determination of the frequency of the light varied according to what we measured (single vs. double source) and how we measured it (baseline vs. source separation). No good explanation has been found, although contamination by extra light in the room is a likely scenario that, unfortunately, cannot be fit for due to uncertainties in the source

Table 4: Frequency Determinations from Each of the 3 Experiment Phases

Phase	Jinc ν (GHz)	Sinc ν (GHz)	cos ν (GHz)
1	13.95 ± 0.28	11.46 ± 0.23	N/A
2	12.78 ± 0.35	10.49 ± 0.29	10.85 ± 0.11
3	N/A	N/A	11.62 ± 0.17

size and characteristic wavelength.

Acknowledgments We gratefully acknowledge Alan Rogers, Preethi Pratap, Phil Shute, and the entire staff of the MIT Haystack Observatory for the use of their facilities and software and their support and instruction. We also thank our instructors, James Moran and Meredith Hughes, for their comments and their help in revising this report. We thank Claude-André Faucher-Giguère for his assistance with our observations.

4. APPENDIX 1

4.1. Projects for the Haystack Trip

Dear Class,

On this coming Thursday, Nov 1, we will go to Haystack for a set of three "hands-on" projects. I think you will find them very interesting and educational! They have been developed over the last ten years as part of Haystack's educational mission, supported by the NSF. The last two projects are new as of this year!

We will have three very knowledgeable staff members from the MIT/Haystack Observatory assisting with the experiments: Dr. Alan Rogers, Dr. Prethi Pratap, and Mr. Phil Shute.

The prime instrument of the Haystack Observatory is a 37-m antenna, which is currently undergoing a major upgrade to operate at 3 mm wavelength. We may be able to see the antenna, which is inside the giant radome.

Alan Rogers told me that they have been picking some local interference at 1420.37 MHz. He is trying to identify it and shut it down. Also, the sun is in behind some geostationary satellites, which also seem to be causing some problems. Hence, you may get to see first hand the problems that radio astronomers have with man-made interference at the low frequency end of the spectrum. Notice that we will be using the unique band around the 21-cm line, which enjoys a very high level of legal protection from interference (There is not supposed to be ANY man-made radiation in the band 1420-1427 MHz)!

Logistics:

*** PLEASE LET ME KNOW RIGHT AWAY WHETHER YOU PLAN TO ATTEND, so I can finalize some of the detailed logistics. Josh Younger cannot come, so we do not have his car. DOES ANYONE ELSE HAVE A CAR??? If not I will rent a van.

We will go regardless of the weather, although it looks like the weather will be perfect (a typical New England Day in the Fall). Remember that water and water vapor cause hardly any attenuation below 2 GHz. Hence, the atmosphere is essentially transparent even during heavy rain. However, if it does rain, bring rain gear because we will be moving around outside.

We will leave the classroom A building entrance at 12:30 sharp and be back by 6 pm. Haystack is in the town of Westford Mass, about 36 miles from the CfA. We will have two vehicles: my car, and (probably) a rented van driven by Meredith. That will handle 12 people. I will bring cookies and drinks.

*** IN THE DESCRIPTION OF THE PROJECTS BELOW, YOU WILL NOTE THAT **ADVANCED PREPARATION ** IS NEEDED FOR EACH PROJECT. PLEASE DIVY UP THE QUESTIONS TO BE RESEARCHED AMONG YOURSELVES. HOWEVER, **** EVERYONE **** NEEDS TO KNOW THE ANSWERS BEFOREHAND. ALSO, PLEASE READ THE THREE ATTACHED ARTICLES, WHICH PROVIDE BACKGROUND FOR THE PROJECTS.

**** TAKE CAREFUL NOTES OF YOUR MEASUREMENTS. YOUR WRITE-UP OF THE RESULTS WILL BE NEXT WEEK'S HOMEWORK.

Three Projects:

1. PROJECT 1: Calibration measurements and observations with a 7.5 foot diameter radio telescope at 1420 MHz.

A. Measure the receiver temperature using the calibrated noise diode and a room temperature absorber.

B. Measure the beamwidth and aperture efficiency of the antenna by observing the Sun.

C. Measure the aperture efficiency on either or both Casseopeia A and Cygnus A. (We may not be able to do this element if the interference is high because the signal strengths are low.)

D. Measure a spectrum of the 21 cm HI line toward the inner galaxy.

A longitude of 30 degrees is probably a good place to look. Look at the attachment srt_20.webarchive to understand how the velocity range of the spectrum a specific longitude tells you what the rotational velocity of the galaxy is at one galactic radii.

The spectral analysis of the signal is done in "firmware" on the processing computer. The bandwidth is 1.25 MHz, and there are 1024 spectral channels. The analysis is not done via autocorrelation function but by direct Fourier transformation of the receiver voltage. No special weighting function is applied, so for the case of uniform weighting the spectral response function will be a sinc^2 function.

PREPARATION:

Read the description of the Small Radio Telescope (SRT) in the attached Sky and Telescope article from 1996 and the attachment entitled srt_20.webarchive.

A. What is the expected beamwidth of the telescope at 1420 MHz?

B. The receiver temperature will probably be about 50K and the bandwidth is 1.25 MHz. What will the approximate continuum sensitivity be in terms of degrees K and Jy for a 1 second integration time?

C. What will the sidereal time be at 3 pm EDT on Nov 1 at Haystack (longitude = 70W)? (This time will be equal to the right ascension of a source transiting then.) (hint, search Google if necessary)

D. What are the coordinates of Cas A and Cyg A and their flux densities at 1420 MHz. Note that the flux density of Cas A is decreasing at a rate of 0.7 percent/year, so a correction will be needed if you find a very old source of information. Will they be above the horizon in the afternoon?

E. What is the temperature and flux density of the sun at 1420 MHz? What is its angular size?

G. What is the exact rest frequency of the 21 cm HI line and what are the approximate magnitudes of the velocity corrections for the rotation of the earth, the orbital motion of the earth, and the peculiar motion of the sun?

H. What is the total bandwidth and spectral resolution at 1420 MHz of the spectrometer in terms of km/s? Is the total velocity width likely to be enough to cover all the galactic hydrogen?

2. PROJECT 2: Measure the fringe visibility of the sun using a two element interferometer at 1420 MHz.

PREPARATION

Read attached memo: VSRT_30.pdf

A. Assume the sun is a uniformly bright circular source. What is the approximate Visibility Function of the Sun at 1420 MHz? What is the baseline spacing in meters for the first null in the visibility function? (see class notes, October 30, 2007). It may be possible to measure deviations from the uniformly bright circular model.

3. PROJECT 3. Play with a lab demonstration setup of a two element interferometer.

The source is two florescent lights (which emit copious amounts of microwaves) to simulate a double radio source .

PREPARATION

Read attached memo: VSRT_25.pdf

A. What is the Visibility Function for a double source? What baseline is needed to reach the first null in the visibility function if the source component separation is b cm and the distance from the source to the interferometer is c cm?

This is gonna be fun!!!!!!!!!!

Jim

5. APPENDIX 2

Astronomy 218
HAYSTACK PROJECT REPORT (aka PS 6)

Due November 13, 2007

5.1. Guidelines for report on measurements made at Haystack on Nov 1, 2007

. Give relevant equations and show data. Please submit final report by Tuesday, Nov 13 at class time and we will discuss the results in class. Make enough copies so everyone has one to refer to.

5.2. PROJECT 1. Calibration and Measurements with a 7.5 ft radio telescope at 1420 MHz.

1. Compare the system temperature measurements derived from the "Y factor" method of putting an ambient temperature absorber in front of the feed with that derived from using the noise diode (with its "calibrated" noise temperature of 100K).

   I believe that the two techniques do not agree very well in their results. Discuss the possible reasons for this. Which do you "believe?"

2. What is the beamwidth of the antenna derived from the sun map? How much is the correction for the finite size of the sun?

3. Calculate the antenna temperature of the sun based on the cal temperature.

4. Compare the result of No. 2 with the one derived if the temperature of the cal is rescaled to make the system temperatures in No. 1 equal.

5. What is the aperture efficiency based on the solar flux density of 5.4×10^5 Jy we obtained from the web for Nov 1?

   How much error does the point source approximation for the sun with respect to the antenna beam introduce in the efficiency calculation?

6. What is the expected flux of the sun based on a brightness temperature of 5800K and an angular size of 30 arcminutes (appropriate for wavelengths shortward of 1 cm)?

   Note how the discrepancy in the system temperature estimates in No. 1 carries over to a discrepancy in the estimated aperture efficiencies (No. 5). In the sociology of the radio astronomer community, the people responsible for the receivers favor calibrations which yield

lower system temperatures, at the expense of lower antenna aperture efficiency, while those responsible for the antenna performance favor calibrations that yield higher aperture efficiency at the expense of the higher system temperatures.

There were several HI profile obtained toward different longitudes. Calculate if possible a piece of the galactic rotation curve, or at least galactic rotation for one radius!

As you can see from SRT memo 20, if you point the telescope along the galactic plane at longitude l, then the line of sight passes closest to the galactic center at the "subcentral point" where the galactic radius is R_s. The highest velocity gas wrt the sun will be at the subcentral point, with a velocity $V_s = V_{max}$. The sun is at radius R_o and is moving with an orbital speed of V_o. Subtracting the sun's velocity from the velocity of gas at R_s, it is easy to show that

$$V(R_s) = V_{max} + V_o \sin l \,, \tag{1}$$

where $R_s = R_o \sin l$.

Assume $V_o = 220$ kms and $R_o = 8$ kpc.

The above analysis holds for longitudes in the "first quadrant," e.g., l between 0 and 90 degrees.

5.3. PROJECT 2. Measure the angular size of the sun with the two element interferometer.

Some critical parameters for the interferometer are its center frequency of 12.825 GHz, and bandwidth of 60 MHz. For the azimuth of the baseline, AZ_B, you should get about 82°, with a baseline length of $D = 3.82$ meters. The baseline length actually changed a bit as a function of azimuth, but ignore this effect.

Alan Rogers sent the two files with the fringe amplitude measured on the sun at 1 second intervals. These were rather large files. I edited them and averaged the data to 6 minutes. The files for day number 305 (our day, November 1) and the previous day (304) are attached.

The columns are:
1. index
2. number of data samples averaged
3. UT time in hrs
4. azimuth angle in degrees
5. elevation angle in degrees
6. fringe amplitude in uncalibrated units.

The data sets have several pecularities.

At some point below 10 degrees elevation the fringe amplitude decreases rapidly because of atmospheric absorption. This effect is worse on Nov 1 because of the heavy cloud cover. For day 304 the antennas were not tracking the sun precisely before about 18.5 hrs. You should disregard this data or bump it up by a factor to match the data, in the mean, on day 305. The interferometer had one fixed delay cable to match the signal delays for a point reached around 18.5 hours UT. For the early part of the tracks you will have to compensate for the delay loss, which is the

$$\sin(2\pi B \cos\psi/c)\,,$$

as derived in class on Nov 6.

1. Calculate the projected baseline length for each data point. The one dimensional estimate from the difference in azimuth angles of the baseline and sun is a good start. But please do the calculation accurately. If ψ is the angle between the baseline vector and the propagation vector to the source then

$$\cos\psi = \sin E_B \sin E_S + \cos E_B \cos E_S \cos(AZ_S - AZ_B)\,, \tag{2}$$

   where
   E_B =elevation angle of baseline vector (assume 0)
   E_S =elevation angle of sun
   AZ_B =azimuth angle of baseline
   AZ_S =azimuth angle of source.

   Remember that I proved a similar relation for $cos\psi$ in celestial polar coordinates in class on Nov 6. The projected baseline is then

$$D_p = D\sin\psi\,, \tag{3}$$

   where D is the distance between the two antennas that you measured.

2. Calculate the effect of the finite bandwidth of the interferometer (60 MHz) on the fringe visibility. Rogers set the delay compensation to be zero at about $UT = 18.5$ hrs. Use the

3. Fit the visibility data (V vs D_p/λ) (corrected for the sinc delay function) to the function of a uniformly bright disk. Don't use data when the since function correction becomes large, e.g., more than say a factor of 2. What is the angular diameter of the radio sun? How does this size compare with the optical diameter? (Consult figure of solar profile and flux vs frequency in the Kraus book, which was distributed during the visit).

4. Can you see any effect of limb brightening in the visibility?

5. Could you Fourier transform the visibility data (actually Hankle transform under assumption of circular symmetry) to produce a radial profile of brightness?

5.4. PROJECT 3. Measure the visibility function of a simulated double source made from two florescent lights.

I know that various sets of data were taken, e.g. fixed source separation, with measurements of fringe amplitude vs baseline; and variable source separation with fringe amplitudes measured at a fixed baseline.

1. Show that the setup confirms the expected response to a double source based on the Fourier transform relation between visibility and baseline.

IMPORTANT NOTE. In both experiments 2 and 3, it is the magnitude of the fringe visibility that is measured (NOT the square of the visibility). Hence this measurement is positive definite. To get the complex visibility it would be necessary to measure the phase of the visibility, which we were not set up to do. If we were, we would have been able to show that the visibility changed sign on alternate extrema.

REFERENCES

[1] Thompson R A, Moran J M, Swendon G W 2004 *Interferometry and Synthesis in Radio Astronomy* (Weinheim: WILEY-VCH Verlag GmbH & Co. KGaA)

[2] `http://www.noaa.gov/`

[3] Kraus, J. D. (1966) *Radio Astronomy* (New York: McGraw-Hill Book Company)